PERGAMON

International Journal of Heat and Mass Transfer 42 (1999) 697–708

International Journal of HEAT and MASS TRANSFER

Condensation heat transfer and pressure drop of refrigerant R-134a in a small pipe

Yi-Yie Yan, Tsing-Fa Lin*

Department of Mechanical Engineering, National Chiao Tung University, Hsinchu, Taiwan 30049, Republic of China

Received 20 January 1998; in final form 5 June 1998

Abstract

The characteristics of condensation heat transfer and pressure drop for refrigerant R-134a flowing in a horizontal small circular pipe that has an inside diameter of 2.0 mm were investigated experimentally in this study. The effects of the heat flux, mass flux, vapor quality and saturation temperature of R-134a on the measured condensation heat transfer and pressure drop were examined in detail. When compared with the data for a large pipe ($D_i = 8.00$ mm) reported in the literature, the condensation heat transfer coefficient averaging over the entire quality range tested here for the small pipe is about 10% higher. Moreover, we noted that in the small pipe the condensation heat transfer coefficient is higher at a lower heat flux, at a lower saturation temperature and at a higher mass flux. In addition, the measured pressure drop is higher for raising the mass flux but lower for raising the heat flux. Based on the present data, empirical correlation equations were proposed for the condensation heat transfer coefficient and friction factors. The results are useful in designing more compact and effective condensers for various refrigeration and air conditioning systems using refrigerant R-134a.

Nomenclature

A heat transfer area [m^2]
Bo boiling number $= q''_w/i_{fg}G$, equation (20)
C_c coefficient of contraction, equation (11)
c_p specific heat [J kg^{-1} °C]
D_i pipe inside diameter [m]
f friction factor
G mass flux [kg m^{-2} s^{-1}]
h heat transfer coefficient [W m^{-2} °C]
i_{fg} enthalpy of vaporization [J kg^{-1}]
k conductivity [W m^{-1} °C]
L length of the pipe tested [m]
Nu Nusselt number
P pressure [MPa]
Pr Prandtl number
Q heat transfer rate [msslW]
q''_w heat flux [W m^{-2}]
Re Reynolds number, dimensionless
Re_{eq} equivalent all liquid Reynolds number, equation (16)
T temperature [K]
v specific volume [m^3 kg^{-1}]
W mass flowrate [kg s^{-1}]
X vapor quality.

Greek symbols

ρ density [kg m^{-3}]
μ viscosity [Ns m^{-2}]
σ contraction ratio
α void fraction.

Subscripts

c cold water side in test section
de deceleration
exp experiment
f friction
fg difference between liquid phase and vapor phase
g vapor phase
i, o at inlet and exit of test section
lat, sens, latent and sensible heats
l liquid phase (assume all flow as liquids)
m average value for the two phase mixture or between the inlet and exit
p pre-evaporator

* Corresponding author

0017–9310/98 $19.00
PII: S0017–9310(98)00195–1

r refrigerant
sat saturated
tp two-phase
w water
wall inner wall of the small pipe.

1. Introduction

To avoid the quick depletion of the Ozone layer in the outer atmosphere above the Antarctic area, various HFC refrigerants have recently been developed to replace the traditional CFC refrigerants. Thus there have been a number of studies reported in the literature to investigate the boiling and condensation heat transfer associated with these HFC refrigerants. The data from these studies are beneficial to the design of the current air conditioners and refrigerators. In attempting to design more compact and effective air conditioning and refrigeration systems for future applications, the heat transfer capacity of the new refrigerants in small tubes with diameter below 0.4 cm needs to be studied. Moreover, among these new refrigerants, R-134a is becoming popular in many applications. In view of these trends in using HFC refrigerants, the present study intends to measure the condensation heat transfer and pressure drop of R-134a flowing in a small circular tube.

In the following the relevant literature on the condensation heat transfer for the new refrigerants is briefly reviewed. Eckels and Pate [1] compared the measured condensation heat transfer coefficient for R-134a and R-12 in an 8.0 mm ID (Inner Diameter) smooth tube. They showed that the condensation heat transfer coefficient for R-134a is 25–35% higher than that for R-12. In addition, the condensation heat transfer coefficients were noted to decrease with the saturated temperature, but increase with the mass flux of the refrigerants. However, the imposed heat flux exhibited little effects on the condensation heat transfer coefficients. In a similar study Torikoshi and Ebisu [2] tested the condensation of R-124a and R-32 and a mixture of R-134a/R-32 in a smooth tube with an ID of 8.7 mm. The condensation heat transfer coefficients for R-134a and R-32 were respectively noted to be about 65 and 10% higher than that for R-22. Besides, the pressure drop for R-134a was larger than that for R-22, but the opposite was the case for R-32. For the mixture of R-134a/R-32 (70 : 30 wt %), the condensation heat transfer coefficient fell below that for R-22, while the pressure drop was larger than that for R-22.

Condensation heat transfer in various enhanced tubes is the topic of several studies. Schlager et al. [3] tested three micro-fin tubes of 9.52 mm OD (Outer Diameter) with R-22. Compared to the smooth tube, the results showed that for condensation heat transfer the enhancement factor was between 1.4 and 1.8, while the pressure drop penalty factor ranged from 1.0 to slightly higher than 1.2. Later, for slightly larger micro-fin tubes the condensation heat transfer enhancement factor was found to be about 1.5–2.0, while the pressure drop penalty had increased by only 20–40% [4]. In a micro-fin tube with 9.52 mm OD, 8.72 mm maximum ID, 17° spiral angle, 60 fins, 0.2 mm fin height, and area ratio of 1.5, Eckels and Pate [5] showed that the condensation heat transfer enhancement factor for R-134a was about 1.8–2.5 and the pressure drop penalty factor was less than the heat transfer enhancement factor. However, in the case at the lowest temperature and highest mass flux, the penalty factor slightly exceeded the enhancement factor. They also noted that the heat transfer coefficient and pressure drop for the micro-fin tubes were lower at a higher saturation temperature. Liu [6] tested a 9.5 mm OD axially grooved tube for R-134a and R-22. He showed that the condensation heat transfer coefficient and pressure drop for R-134a were respectively 8 and 18% and were 50% higher than those for R-22. Similar studies were conducted for shell side condensation of R-134a [7–9]. Huber et al. [7] studied the condensation for two kinds of fin density. Their results showed that the 40-fpi tube performs better than the 26-fpi tube. Later, two enhanced tubes—one was the tube G-SC with long, Y-shaped fins, and the other was the tube Tu-Cii with short fins roughened by mechanical working—were tested [8]. The results showed that the Tu-Cii tube performed better than the G-SC tube. They concluded that the Tu-Cii tube was significantly better than the other tubes tested. However, the G-SC tube was only slightly better than the 26-fpi tube. In a continuing study [9] they further showed that R-134a performed better than R-12. Moreover, for both R134-a and R-12 the condensation heat transfer coefficients for all the above tube geometries dropped with increasing heat flux. Recently, some advanced micro-fin tubes with cross-groove geometries were tested for R-22 by Chamra and Webb [10]. They found that the tubes had about 27% higher condensation heat transfer coefficient than the single-helix tube, while the pressure drop was only 6% higher.

The studies reviewed above are for tubes with a diameter larger than 6 mm. Recently, Yang and Webb [11] tested two flat extruded small aluminium tubes with cross section of 16 mm in width and 3 mm in height. They were separated into four parallel channels by three membranes. The hydraulic diameters are 2.637 and 1.564 mm, respectively, corresponding to the smooth and micro-fin tubes. The refrigerant R-12 was tested with the mass flux ranging from 400 to 1400 kg m^{-2} s^{-1}. The condensation heat transfer coefficient was noted to increase with the mass velocity and vapor quality but decrease with the heat flux for both tubes. Two correlation equations proposed by Shah [12] and Akers et al. [13] shows better agreement with their data. The correlation from Akers et al. [13] were compared with their

data. Furthermore, they indicated that for the vapor quality higher than 0.5, the surface tension drainage force becomes effective and provided additional enhancement to the condensation heat transfer for the micro-fin tube. Meanwhile, Yang and Webb [14] measured the friction factor for the tubes. The results showed that, for single-phase liquid, the friction factors for the plain and micro-fin tubes were respectively 14 and 36% higher than that predicted by the Blasius equation. For two-phase flow, the pressure gradient was found to increase with the mass velocity and vapor quality. The pressure gradient in the micro-fin tube was higher than that for the plain tube. With the concept of an equivalent mass velocity which was first proposed by Akers et al. [13], a very good single curve was obtained in correlating the data for the plain and micro-fin tubes.

The above literature review clearly indicates that the heat transfer and pressure drop data for the condensation of R-134a in small tubes having a diameter smaller than 4 mm are not available. In this study, the characteristics of condensation heat transfer and pressure drop for refrigerant R-134a flowing in a small pipe of 2 mm inside diameter were explored experimentally. Comparison of the measured heat transfer coefficient for this small pipe with that for a larger pipe was conducted. Moreover, correlation equations for the heat transfer coefficient and pressure drop for this small pipe were proposed.

2. Experimental apparatus and procedures

The experimental apparatus established in the present study schematically shown in Fig. 1 consists of four main loops and a data acquisition system. More specifically, the apparatus includes a refrigerant loop, a water loop for a pre-evaporator, a water loop for a test section and a water–glycol loop. Refrigerant R-134a is circulated in the refrigerant loop. We need to control the temperatures and flowrates in the water loop for the pre-evaporator and in the water–glycol loop to obtain the preset inlet vapor quality and pressure of the refrigerant in the test section in the refrigerant loop. Meanwhile, the water loop for the test section is adjusted to achieve the required mean output heat flux from the small tubes in the test section.

2.1. Refrigerant loop

The refrigerant loop contains a refrigerant pump, an accumulator, a mass flow-meter, a pre-evaporator, a test section, a condenser, a sub-cooler, a receiver, a filter-dryer and three sight glasses. The refrigerant pump is driven by a DC motor which is in turn controlled by a variable DC output motor controller. The liquid flowrate of R-134a is varied by a rotational DC motor through changing the DC current. The refrigerant flowrate can be further adjusted by opening the by-pass valve. In the loop the accumulator is used to dampen the fluctuations of the flowrate and pressure. The refrigerant flowrate is measured by a mass flow meter with an accuracy of $\pm 1\%$. The pre-evaporator is used to evaporate the refrigerant R-134a to a specified vapor quality at the test section inlet by receiving heat from the hot water in the water loop. Note that the amount of heat transfer from the hot water to the refrigerant in the pre-evaporator is calculated from the energy balance in the water flow. Meanwhile, a condenser and a sub-cooler are used to condense the refrigerant vapor from the test section by the cold water–glycol loop. The pressure of the refrigerant loop can be controlled by varying the temperature and flowrate of the water–glycol in the condenser. After condensation, the liquid refrigerant flows back to the receiver.

2.2. Test section

In view of the pipe to be tested being relatively small, the refrigerant flowrate in it is very small and direct measurement of the condensation heat transfer coefficient and pressure drop is difficult and subject to large error. Thus 28 small pipes, each having the same diameter and length, are put together to form the test section, as shown in Fig. 2(a). Each small pipe has an inside diameter of 2.0 mm, outside diameter of 3.0 mm and length of 0.2 m. Specifically, these 28 pipes are placed together side by side forming a plane bundle. At the middle axial station of the pipes 10 thermocouples are soldered on the outer surfaces of the pipes. These thermocouples are soldered on 10 selected pipes at circumferential positions of 45° from the top of the pipe or from the bottom of the pipe, as shown in Fig. 2(b). Two copper plates, each 5 mm thick, are soldered in the upper and lower sides of the pipe bundle. The width of each copper plate is the same as the pipe bundle but it was only 0.1 m long. Obviously small crevices exist between the pipe outside surface and copper plates. Therefore the thermocouple wires are placed along these crevices. Due to the good thermal contact of the copper plates and the pipes, there is no need to fill the crevices with conducting grease. Instead, the crevices provide the space for the thermocouple wires leading to the data logger Each copper plate is in turn covered with another plane pipe bundle consisting of 10 pipes. These pipes have the same outside diameter of 10 mm and are soldered side by side and soldered onto the copper plates, as shown in Fig. 2(a). Cold water form a low temperature thermostat is allowed to flow through these two pipe bundles which act as heat sinks, to remove the heat from the R-134a condensation in the small pipes. The flowrates and temperatures in the two bundles are controlled at the same level. To reduce the heat loss of the test section, the whole test section is wrapped in 10 cm thick polyethylene. Care is taken to design the inlet

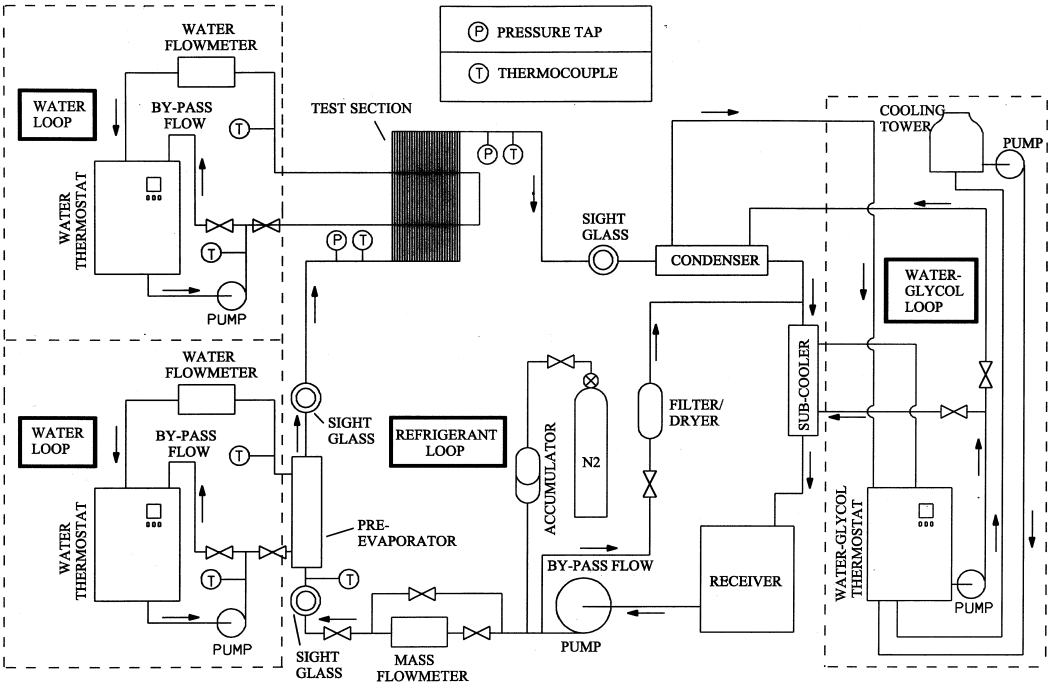

Fig. 1. Schematic diagram of the experimental system.

and outlet of the connection pipe to the refrigerant pipe bank so that the R-134a flowrate in each small pipe is nearly the same. The refrigerant pressure and pressure drop at and across the pipe inlet and exit are measured by the pressure transducers all having the same accuracy of $\pm 1\%$.

2.3. Water loop for test section

The water loop in the experimental apparatus for circulating the cold water through the test section contains a 80 l constant temperature water bath with a 4 kW heater and an air cooled refrigeration system of 3.5 kW cooling capacity intended to control the water temperature. A 0.5 hp water pump with an inverter is used to drive the cold water to the test section with a specified water flowrate. A by-pass valve can also be used to adjust the water flowrate. the accuracy of measuring the water flowrate is $\pm 0.5\%$.

2.4. Water loop for pre-evaporator

The water loop designed for the pre-evaporator consists of a 125 l constant temperature hot water bath with three 2.0 kW heaters in it and a 0.5 hp water pump to drive the hot water at specified temperature and flowrate to the pre-evaporator. The pre-evaporator is a double pipe heat exchanger having a heat transfer area of 0.12 m^2. The pre-evaporator and the connection pipe between the test section and the pre-evaporator were thermally well insulated with 6 cm thick polyethylene. Similarly, a by-pass valve is also used to adjust the water flowrate. The water flowmeter also has an accuracy of $\pm 0.5\%$.

2.5. Water–glycol loop

The water–glycol loop designed for condensing the R-134a vapor contains a 125 l constant temperature bath with a low temperature water–glycol mixture circulating through the subcooler. The cooling capacity is 2 kW for the mixture at $-20^{\circ}C$. The cold water–glycol mixture at a specified flowrate is driven by a 0.5 hp pump to the condenser as well as to the sub-cooler. A by-pass valve is also provided to adjust the flowrate.

2.6. Data acquisition

The data acquisition system includes a recorder, a 24 V-3 A power supply and a controller. The recorder is used to record the temperature and voltage data. The water flowmeters and differential pressure transducers need a 24 V power supply as a driver to output an electric current of 4 to 20 mA. The IEEE488 interface is used to connect the controller and the recorder, allowing the measured data to transmit from the recorder to the controller and then analyzed by the computer immediately.

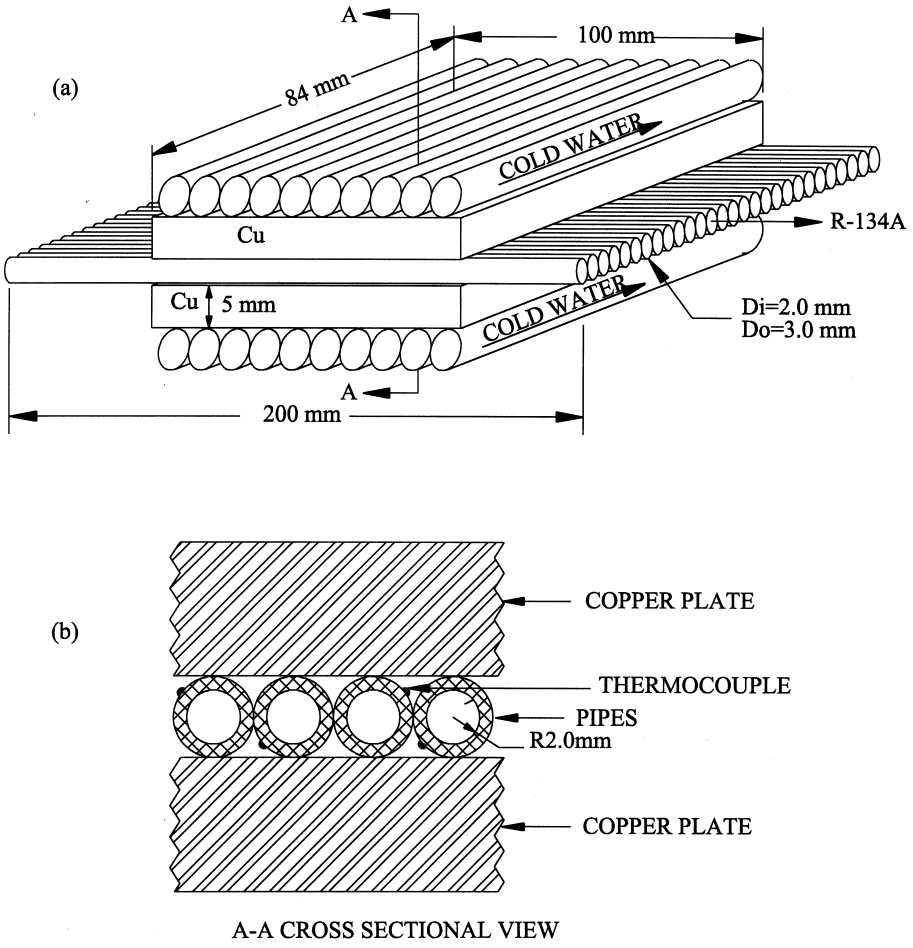

Fig. 2. (a) Test section of the small pipes and (b) locations of the thermocouples.

2.7. Experimental procedures

In the test, the R-134a pressure at the test section inlet is first maintained at a specified level by adjusting the water-glycol temperature and its flowrate. Then, the temperature and flowrate of the hot water loop for the pre-evaporator are adjusted to keep the vapor quality of R-134a at the test section inlet at the desired value. Finally, the heat transfer rate from the R-134a condensation in the small pipes to the cold water bundles above and below it is adjusted by changing the temperature and flowrate of the cold water loop for the test section. Note that the above procedures need to be adjusted iteratively to obtain a preset condition in the test section. By measuring the enthalpy change of the water between the inlet to the exit of the pipe bundles covering the copper plates in the test section, we can calculate the amount of the heat transfer from the refrigerant R-134a.

3. Data reduction

An analysis is needed to calculate the condensation heat transfer coefficient and friction factor from the experimental data. This data reduction process is described in the following.

3.1. Single phase heat transfer

Before measuring the condensation heat transfer coefficient and pressure drop, an initial single phase heat transfer test was conducted to check the energy balance in the test section. The results indicated that the energy balance between the water and refrigerant sides was within 2% for all runs. This insures the heat loss from the test section being rather small and the test section being appropriate for our measurement.

3.2. Two-phase condensation heat transfer

The vapor quality of the R-134a at the test section inlet was evaluated from the energy balance for the pre-evaporator. Based on the temperature drop on the water side in the pre-evaporator, the total heat transfer rate from the water to the refrigerant can be calculated from the relation

$$Q_{w,p} = W_{w,p} c_{p,w} (T_{w,p,i} - T_{w,p,o}) \tag{1}$$

This heat transfer to the refrigerant in the pre-evaporator causes its temperature to rise to the saturated value (a sensible heat transfer process) and then causes the refrigerant to evaporate (a latent heat transfer process). Thus

$$Q_{w,p} = Q_{sens} \text{ and } Q_{lat} \tag{2}$$

where $Q_{sens} + Q_{lat}$ are respectively the total sensible and latent heat transfer rates of the R-134a in the pre-evaporator, and

$$Q_{sens} = W_r c_{p,r} (T_{r,sat} - T_{r,p,i}) \tag{3}$$

$$Q_{lat} = W_r i_{fg} X_{p,o} \tag{4}$$

The above equations can be combined to evaluate the refrigerant vapor quality at the exit of the pre-evaporator, that is considered to be the same as the vapor quality of the refrigerant entering the test section. Specifically,

$$X_i = X_{p,o} = \frac{1}{i_{fg}} \left[\frac{Q_{w,p}}{W_r} - c_{p,r} (T_{r,sat} - T_{r,p,i}) \right] \tag{5}$$

The total change of the refrigerant vapor quality in the test section was then deduced from the total heat transfer rate from the refrigerant side to the cold water side in the test section $Q_{w,c}$,

$$\Delta X = \frac{Q_{w,c}}{W_r i_{fg}} \tag{6}$$

where $Q_{w,c}$ is estimated from the measured total temperature rise in the cold water side in the test section. Finally, the average heat transfer coefficient for the condensation of R-134a in the test section was determined from the definition

$$h_r \equiv \frac{Q_{w,c}}{A(T_r - T_{wall})} \tag{7}$$

where T_{wall} is the average of the measured pipe wall temperatures at the detected locations and T_r is the refrigerant temperature which is, in turn, estimated from the measured refrigerant temperatures at the upstream of the inlet and downstream of the exit of the test section, which are nearly the same as the saturation temperatures corresponding to the pressures detected from these locations. Thus

$$T_r = \frac{(T_{r,i} + T_{r,o})}{2} \tag{8}$$

3.3. Friction factor

Note that in the condensation of R-134a in the pipes, the flow decelerates and pressure rises as it moves downstream. Besides, the refrigerant pressure also drops for the flow contraction at the inlet and rises for the flow expansion at the exits of the small pipes. Thus, in the refrigerant side the two phase friction pressure drop ΔP_f associated with the R-134a condensation was calculated by adding the deceleration pressure increase ΔP_{de} and the pressure rise at the test section exit ΔP_o to and by subtracting the pressure drop at the test section inlet ΔP_i from the measured total pressure drop ΔP_{exp}.

$$\Delta P_f = \Delta P_{exp} + \Delta P_{de} + \Delta P_o - \Delta P_i \tag{9}$$

The deceleration pressure increase was estimated by the homogeneous model for two phase gas–liquid flow [15] as

$$\Delta P_{de} = G^2 v_{fg} \Delta X \tag{10}$$

Moreover, the sudden contraction pressure drop and expansion pressure rise, ΔP_i and ΔP_o for the two phase flow associated with the inlet and exit ports estimated by Collier [15] based on a separated flow model were chosen here and they are

$$\Delta P_i = \left(\frac{G}{C_c} \right)^2 (1 - C_c) \times \left[\frac{(1 + C_c)[X_m^3 v_g^2/\alpha^2 + (1 - X_m)^3 v_l^2/(1-\alpha)^2]}{2[X_m v_g + (1 - X_m) v_l]} - C_c \left[\frac{X_m^2 v_g}{\alpha} + \frac{(1 - X_m)^2 v_g}{(1-\alpha)} \right] \right) \tag{11}$$

$$\Delta P_o = G^2 \sigma (1 - \sigma) v_l \left[\frac{(1 - X_m)^2}{(1-\alpha)} + \left(\frac{v_g}{v_l} \right) \frac{X_m^2}{\alpha} \right] \tag{12}$$

where C_c in equation (11) is the coefficient of contraction and is a function of the contraction ratio σ. The void fraction α in the above equations was correlated by Zivi [16] as

$$\alpha = \frac{1}{1 + \left(\frac{1 - X_m}{X_m} \right) \left(\frac{\rho_g}{\rho_l} \right)^{2/3}} \tag{13}$$

Based on the above estimation the acceleration pressure drop and the pressure losses at the inlet and exit ports are rather small and the frictional pressure drop ranges from 95 to 98% of the total pressure drop measured. In addition, for two-phase flow Yang and Webb [14]

introduced an equivalent all-liquid mass flux G_{eq} to replace the convectional mass flux G in defining the friction factor. The equivalent all-liquid mass flux G_{eq} was originally proposed by Akers et al. [13] as

$$G_{eq} = G\left[(1-X_m)+X_m\left(\frac{\rho_l}{\rho_v}\right)^{0.5}\right] \tag{14}$$

The two phase friction factor is then defined as

$$f_{tp} \equiv \frac{\Delta P_f}{G_{eq}^2/2\rho_l}\frac{D_i}{4L} = \frac{\Delta P_f}{Re_{eq}^2\mu_l^2/2\rho_l}\frac{D_i}{4L} \tag{15}$$

where the equivalent all-liquid Reynolds number Re_{eq} is defined as

$$Re_{eq} = \frac{G_{eq}D_i}{\mu_l} \tag{16}$$

3.4. Uncertainty analysis

The analysis of the uncertainties for the present experimental results was determined by the procedures proposed by Kline and McClintock [17]. The detailed results from the present uncertainty analysis for the experiments conducted here are summarized in Table 1.

4. Results and discussion

To check the suitability of the above experimental system for the present measurement, the single phase liquid R-134a heat transfer data were measured first and compared with the well-known correlations from Dittus–Boelter [12] and Gnielinski [18] in Fig. 3. The Dittus–Boelter correlation is

$$Nu = 0.023Re^{0.8}Pr^{0.4} \tag{17}$$

and the Gnielinski correlation is

$$Nu = \frac{(f/2)(Re-1000)Pr}{1+12.7\sqrt{f/2}(Pr^{2/3}-1)}[1+(D_i/L)^{2/3}](Pr/Pr_w)^{0.11} \tag{18}$$

where Pr_w is the Prandtl number of the R-134a liquid at the pipe wall temperature and f is the friction factor which was calculated by the Blasius equation. The Blasius equation is

$$f = 0.079Re^{-1/4} \tag{19}$$

The comparison indicated that our experimental results are in reasonable agreement with the Dittus–Boelter and Gnielinski correlations for the mass flux G above 200 kg m^{-2} s^{-1}. At $G < 200$ kg m^{-2} s^{-1} the experimental results depart significantly from those calculated by the two correlations. This is the consequence of the fact that at $G < 200$ kg m^{-2} s^{-1} the corresponding Reynolds number in the small pipe studied here is lower than 2000 and the flow is laminar. Figure 4 shows the corresponding single phase liquid R-134a friction factor variation with the Reynolds number. The results indicate that our measured friction factor is substantially higher than the data for a smooth pipe estimated by the Blasius equations. But they have a similar trend. The higher friction factor in our pipes can be attributed to the significant hydrodynamic entrance effect in the short pipes ($L/D_i = 100$) considered and the roughness of the inside surfaces of these pipes. Through the above comparison the present experimental

Table 1
Parameters and estimated uncertainties

Parameter	Uncertainty
Length, width and thickness [m]	±0.5%
Area [m^2]	±1%
Temperature, T (°C)	±0.2°C
ΔT (°C)	±0.3°C
Pressure, P (MPa)	±0.002 MPa
Pressure drop, DP (Pa)	±200 Pa
Water flowrate, $W_{w,c}$ and $W_{w,p}$	±2%
Mass flux of refrigerant, G	±2%
Heat transfer rate of test section, Q_h	±3%
Heat transfer rate of pre-evaporator, $Q_{w,p}$	±3%
Vapor quality, X	±0.03
Single liquid phase heat transfer coefficient, h	±10%
R134-a condensation heat transfer coefficient, h_r	±15%
Two-phase friction factor, f_{tp}	±20%

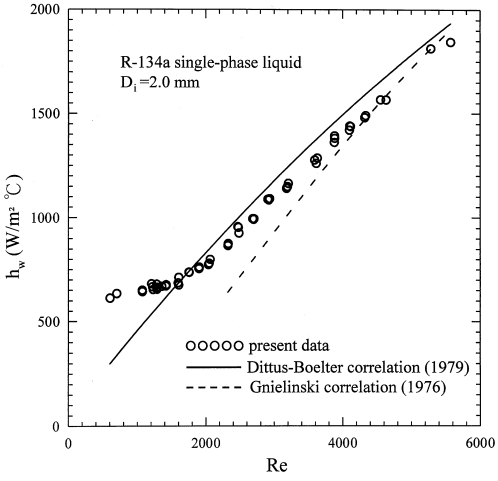

Fig. 3. Comparison of the present data for the liquid phase heat transfer coefficient with the Dittus–Boelter and Gnielinski correlations.

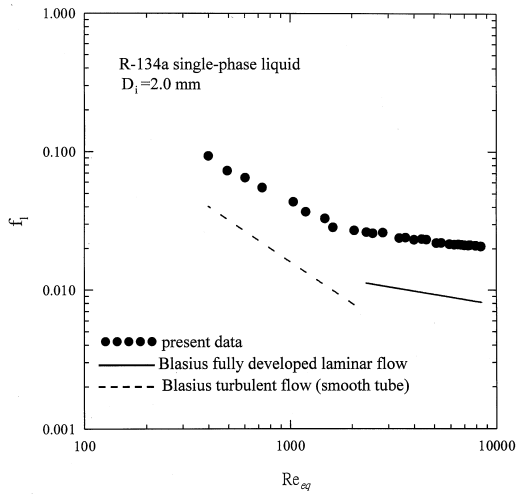

Fig. 4. Variations of the present single-phase liquid friction factor with the Reynolds number and comparison of the data with the Blasius equations for fully developed laminar flow and turbulent flow.

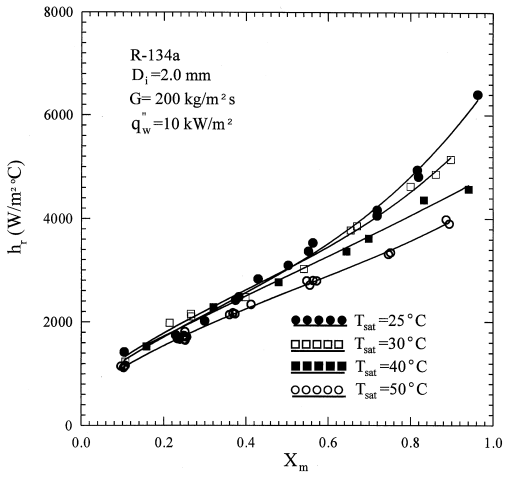

Fig. 5. Effects of the refrigerant saturated temperature on the condensation heat transfer at $G = 200$ kg m^{-2} s^{-1} and $q''_w = 10$ kW m^{-2}.

design is considered to be suitable for the present measurement of two phase condensation heat transfer and pressure drop. After this single phase test we started to investigate the effects of various parameters, namely, the mass flux, heat flux and saturated temperature, on the two-phase condensation flow. In what follows only a small sample of the results obtained is presented to illustrate these effects.

4.1. Two-phase condensation heat transfer

The effect of the refrigerant saturated temperature (pressure) on the condensation heat transfer coefficient is illustrated in Fig. 5 by presenting the data for four typical cases at $q''_w = 10$ kw m^{-2} and $G =$ kg m^{-2} s^{-1} at different mean vapor qualities for T_{sat} ranging from 25 to 50°C. The results suggest that at a given saturated temperature the condensation heat transfer coefficient rises significantly with the mean vapor quality especially at a lower T_{sat}. While at a fixed X_m the condensation heat transfer coefficient is poorer at a higher T_{sat} especially in the high quality region, $X_m > 0.6$. According to the energy transport mechanisms in the condensing flow, the overall heat transfer for the condensation of R-134a flow in the pipes is mainly dominated by the thermal resistance associated with the convection at the vapor–liquid interface. Note that at a high vapor quality the vapor moves at a higher speed and the interfacial condensation is higher. Thus the heat transfer increases with the vapor quality. On the other hand, at a higher saturated temperature the thermal conductivity of the liquid R-134a is lower and the associated thermal resistance of the liquid film is larger, causing a poorer heat transfer rate.

Next, the effect of the average wall heat flux on the condensation heat transfer is shown in Fig. 6 by presenting the heat transfer data for two heat fluxes of 10 and 20 kW m^{-2} at $T_{sat} = 40$°C and $G = 100$ and 200 kg m^{-2} s^{-1}. It is well known that the condensation rate would be proportional to the wall heat flux. However, the results indicate that the condensation heat transfer coefficient is lower for a higher heat flux for a given mass flux except in the low vapor quality region, $X_m < 0.2$ for $G = 200$ kg m^{-2} s^{-1}. This reflects that the vapor condensation rate can be enhanced by a smaller amount when compared with an increase in the temperature difference between the refrigerant and the cold water in the test section. This means that more proportional

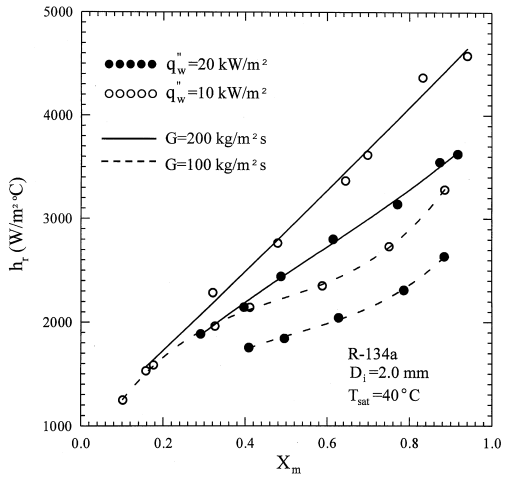

Fig. 6. Effects of the heat flux on the condensation heat transfer for $T_{sat} = 40$°C.

demanding of the temperature gradient at the interface between the wall and the flow is needed to achieve a higher heat flux.

The effect of the refrigerant mass flux on the condensation heat transfer is exemplified in Fig. 7 for $q''_w = 10$ kW m^{-2} and $T_{sat} = 40°C$. The results show that in the high vapor quality region for $X_m \geqslant 0.5$ the heat transfer coefficient increases with the mass flux. But at a low quality with $X_m < 0.3$ the heat transfer coefficient is only slightly affected by the mass flux. Note that at a low quality the vapor flow is slow and the second phase is stratified [15]. For the stratified flow the velocity of the liquid induced from the shear force associated with the low vapor flow is limited. Thus, the differences in the condensation rates for different mass fluxes are limited. While for the high vapor quality region the vapor flow is at a high speed and the annular flow pattern prevails in the pipe. For the annular flow the condensation heat transfer would clearly be influenced by the flow in the vapor core.

Finally, it is important to compare the present data for the R-134a condensation heat transfer in a small pipe to those in large pipes reported in the literature. Due to the limited availability of the data for large pipes with a similar range of parameters covered in the present study, the comparison is only possible for a few cases. This is shown in Fig. 8, in which our data are compared with those from Eckels and Pate [1]. Note that the results from Eckels and Pate [1] are average h_r values measured in a long pipe of 3.67 m in length with the vapor quality varying from 0.9 at the pipe inlet to 0.1 at the exit. But in the present test the pipe is rather short, 10 cm in length, and the total quality change in the entire pipe is very small. The comparison clearly shows that as the quality X_m is approximately above 0.4 the small pipe has better

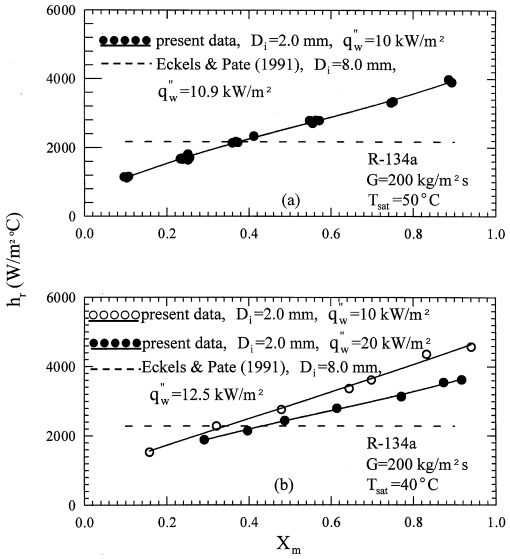

Fig. 8. Comparison of the present heat transfer data with those for the larger pipe from Eckels and Pate (1991).

condensation heat transfer. But the opposite is the case for a low vapor quality with $X_m < 0.3$. When averaging over the entire quality range tested here the condensation heat transfer coefficient for the small pipe is about 10% higher than the large pipe with $D_i = 8.0$ mm.

4.2. Two-phase pressure drop

The frictional pressure drops associated with the R-134a condensation in the small pipe under various flow and thermal conditions are presented in Figs 9–11. The

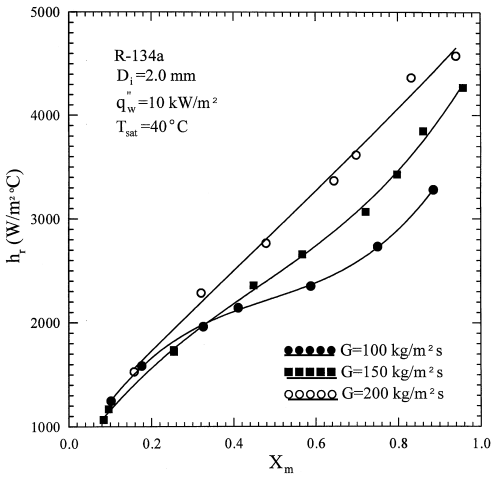

Fig. 7. Effects of the mass flux on the condensation heat transfer at $q''_w = 10$ kW m^{-2} and $T_{sat} = 40°C$.

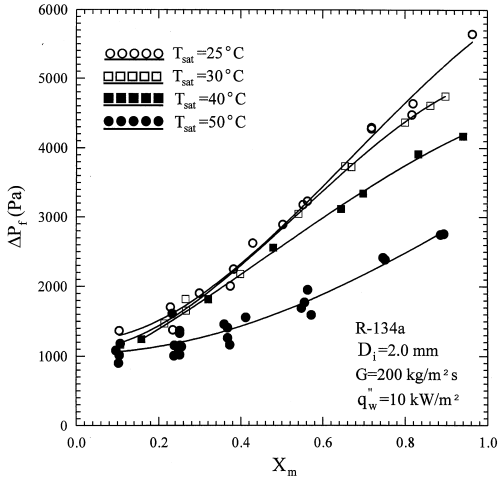

Fig. 9. Frictional pressure drop variations with the mean vapor quality at various refrigerant saturated temperatures at $G = 200$ kg m^{-2} s^{-1} and $q''_w = 10$ kW m^{-2}.

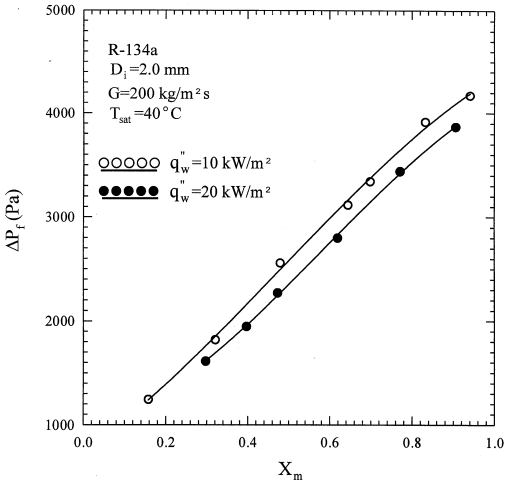

Fig. 10. Frictional pressure drop variations with the mean vapor quality for two different heat fluxes at $G = 200$ kg m^{-2} s^{-1} and $T_{sat} = 40°C$.

results in Fig. 9 for different saturation temperatures of R-134a indicate that at a given T_{sat} the pressure drop is larger for a higher vapor quality. This pressure drop increase with the quality is more pronounced for a lower saturation temperature. Note that except in the low vapor quality range the pressure drop gets smaller at a higher T_{sat} especially when T_{sat} is raised from 40 to 50°C. This trend is similar to the effect of T_{sat} on the condensation heat transfer coefficient examined in Fig. 5. Moreover, Fig. 10 suggests that an increase in the heat flux results in a mild decrease of the frictional pressure drop and the variation is also similar to that in Fig. 6 for the change of the condensation heat transfer with the heat flux. We further note that the effect of the mass flux on the frictional pressure drop shown in Fig. 11 is similar to the trend in the heat transfer coefficient change with the mass flux shown in Fig. 7. The results in Fig. 11 indicate that at a given mass flux the pressure drop is larger for a higher vapor quality. In addition, the pressure drop increase with the quality is more pronounced for a higher mass flux.

4.3. Correlation equations

Correlation equations for the heat transfer coefficient and friction factor associated with the R-134a condensation in the small pipe considered here are important in the future practical thermal design of the compact condensers in various air conditioning and refrigeration systems. An equivalent Reynolds number, regarding the entire flow as liquid proposed by Akers et al. [13] already defined in equation (16), along with the boiling number are chosen to correlate the measured data. The boiling number is defined as

$$Bo = \frac{q''_w}{i_{fg}G} \tag{20}$$

Based on the present data for various heat fluxes and mass fluxes, a condensation heat transfer correlation for R-134a in the small pipe was proposed as

$$\frac{h_r D_i}{k_l} Pr_l^{-0.33} Bo^{0.3} Re = 6.48 Re_{eq}^{1.04} \tag{21}$$

Figure 12 shows the comparison of the present data with the correlation. The average deviation between the present data and the correlation is about 9.2%. Similarly,

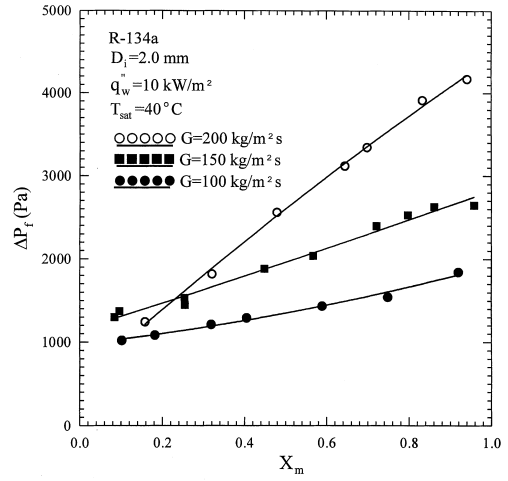

Fig. 11. Frictional pressure drop variations with the mean vapor quality at various mass fluxes for $q''_w = 10$ kW m^{-2} and $T_{sat} = 40°C$.

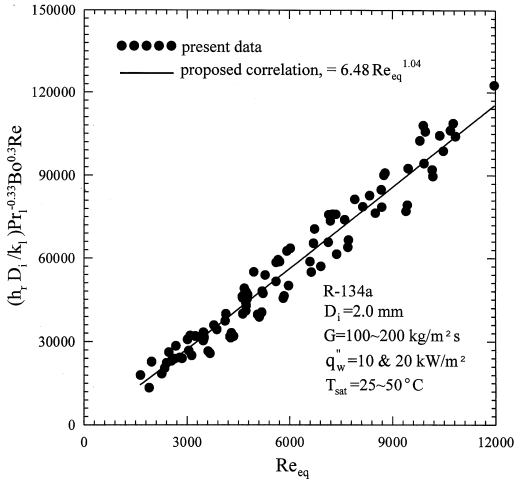

Fig. 12. Variations of the measured two phase dimensionless heat transfer coefficient with the equivalent Reynolds number and compared with the proposed correlation.

based on the present data, the friction factor is correlated as

$$f_{tp} = 498.3 Re_{eq}^{-1.074} \quad (22)$$

with an average deviation about 16.6%, as shown in Fig. 13.

5. Concluding remarks

An experiment has been carried out in the present study to measure the heat transfer coefficient and pressure drop for the condensation of R-134a flowing in a small pipe of 2 mm in diameter. The present results for the small pipe indicate that the condensation heat transfer coefficient and pressure drop are lower at a higher saturated temperature of the refrigerant. For a higher heat flux the condensation heat transfer coefficient and pressure drop are lower for the entire vapor quality range tested here. The mass flux exhibits different effects to the heat transfer coefficient at different vapor qualities. In the low vapor quality region the mass flux shows slight influence, but in the high vapor quality region the heat transfer coefficient and pressure drop increase significantly, with the mass flux. Moreover, the condensation heat transfer coefficient averaged over the entire quality range tested for the small pipe is about 10% higher than that for the large pipe with $D_i = 8.0$ mm. Finally, for practical application, empirical correlations were proposed to correlate the present data for the heat transfer coefficient and friction factor in the small pipe.

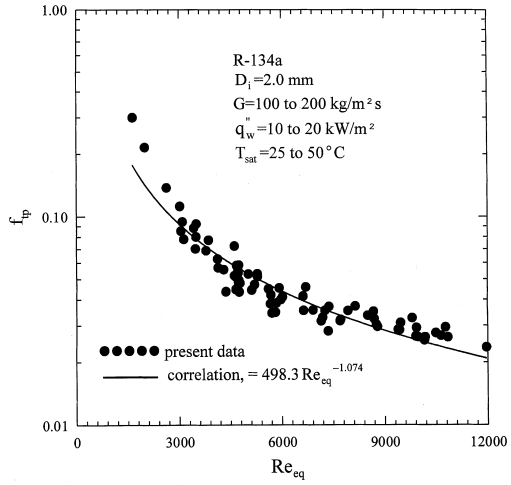

Fig. 13. Variations of the measured two phase friction factor with the equivalent Reynolds number and compared with the proposed correlation.

Acknowledgements

The financial support of this study by the engineering division of National Science Council of Taiwan, Republic of China through the contract NSC85-2221-E-009-046 and Dr B.C. Yang's help during construction of the present experimental facility are greatly appreciated.

References

[1] S.J. Eckels, M.B. Pate, An experimental comparison of evaporation and condensation heat transfer coefficients for HFC-134a and CFC-12, Int. J. Refrig. 14 (1991) 70–77.
[2] K. Torikoshi, T. Ebisu, Heat transfer and pressure drop characteristics of R-134A, R-32 and a mixture of R-32/R-134A inside a horizontal tube, ASHRAE Trans. 99 (1993) 90–96.
[3] L.M. Schlager, M.B. Pate, A.E. Bergles, Heat transfer and pressure drop during evaporation and condensation of R22 in horizontal micro-fin tubes, Int. J. Refrig. 12 (1989) 6–14.
[4] L.M. Schlager, M.B. Pate, A.E. Bergles, Evaporation and condensation heat transfer and pressure drop in horizontal, 12.7-mm microfin tubes with Refrigerant 22, J. Heat Transfer 112 (1990) 1041–1047.
[5] S.J. Eckels, M.B. Pate, Evaporation and condensation of HFC-134a and CFC-12 in a smooth tube and a micro-fin tube, ASHRAE Trans. 97 (1991) 71–81.
[6] X. Liu, Condensing and evaporating heat transfer and pressure drop characteristics of HFC-134a and HCF-C-22, J. Heat Transfer 119 (1997) 158–163.
[7] J.B. Huber, L.E. Rewerts, M.B. Pate, Shell-side condensation heat transfer of R-134a—part I: finned-tube performance, ASHRAE Trans. 100 (2) (1994) 239–247.
[8] J.B. Huber, L.E. Rewerts, M.B. Pate, Shell-side condensation heat transfer of R-134a—part II: enhanced tube performance, ASHRAE Trans. 100 (2) (1994) 248–256.
[9] J.B. Huber, L.E. Rewerts, M.B. Pate, Shell-side condensation heat transfer of R-134a-part III: comparison with R-12, ASHRAE Trans. 100 (2) (1994) 248–256.
[10] L.M. Chamra, R.L. Webb, Advanced micro-fin tubes for condensation, Int. J. Heat Mass Transfer 39 (1996) 1839–1846.
[11] C.-Y. Yang, R.L. Webb, Condensation of R-12 in small hydraulic diameter extruded aluminium tubes with and without micro-fins, Int. J. Heat Mass Transfer 39 (1996) 791–800.
[12] M.M. Shah, A general correlation for heat transfer during film condensation inside pipes, Int. J. Heat Mass Transfer 22 (1979) 547–556.
[13] W.W. Akers, H.A. Deans, O.K. Crosser, Condensation heat transfer within horizontal tubes, Chem. Eng. Prog. 54 (1958) (10) 89–90.
[14] C.-Y. Yang, R.L. Webb, Friction pressure drop of R-12 in small hydraulic diameter extruded aluminium tubes with and without micro-fins, Int. J. Heat Mass Transfer 39 (1996) 801–809.
[15] J.G. Collier, Convective Boiling and Condensation, 2nd

ed., McGraw-Hill International Book Company, 1982, pp. 32, 90–93, 341.

[16] S.M. Zivi, Estimation of steady state steam void-fraction by means of principle of minimum entropy production, J. Heat Transfer 86 (1964) 237–252.

[17] S.J. Kline, F.A. McClintock, Describing uncertainties in single-sample experiments, Mech. Eng. 75 (1) (1953) 3–12.

[18] V. Gnielinski, New equations for heat and mass transfer in turbulent pipe and channel flow, Int. Chem. Eng. 16(2) (1976) 359–367.